JGR Earth Surface

RESEARCH ARTICLE
10.1029/2020JF005545

Low Dust Generation Potential From Active Sand Grains by Wind Abrasion

N. Swet[1], J. F. Kok[2], Y. Huang[2], H. Yizhaq[3], and I. Katra[1]

[1]Department of Geography and Environmental Development, Ben Gurion University of the Negev, Beersheba, Israel, [2]Department of Atmospheric and Oceanic Sciences, University of California, Los Angeles, CA, USA, [3]Department of Solar Energy and Environmental Physics, BIDR, Ben-Gurion University of the Negev, Beersheba, Israel

Key Points:
- Wind tunnel experiments on noncoated sand provide first quantitative information of dust emission from abrasion under saltation conditions
- The study presents a comparison between the different dust emission mechanisms from active sand and nonsandy soils
- Aeolian sand abrasion was found to have only low potential to generate dust particles

Supporting Information:
- Supporting Information S1

Correspondence to:
N. Swet,
swet@post.bgu.ac.il

Citation:
Swet, N., Kok, J. F., Huang, Y., Yizhaq, H., & Katra, I. (2020). Low dust generation potential from active sand grains by wind abrasion. *Journal of Geophysical Research: Earth Surface*, *125*, e2020JF005545. https://doi.org/10.1029/2020JF005545

Received 27 JAN 2020
Accepted 31 MAY 2020

Author Contributions:
Conceptualization: J. F. Kok, I. Katra
Formal analysis: N. Swet, Y. Huang, H. Yizhaq
Methodology: N. Swet
Writing - original draft: N. Swet
Writing – review & editing: N. Swet, J. F. Kok, Y. Huang, H. Yizhaq, I. Katra

Abstract Wind-driven dust emission has a major impact on many environmental and socioeconomic issues such as climate change, soil loss, biogeochemical cycles, and air pollution. It is generally assumed that the main global dust sources consist of nonsandy soils with high percentages of fine-sized clay and silt particles. However, in recent years, it has been hypothesized that active sand bodies can generate significant dust emissions through the mechanism of sand abrasion. Moreover, sand abrasion has been used to explain the formation of certain soils on Earth and Mars. Here, we test the hypothesis that sand abrasion can generate substantial dust emissions by performing targeted wind tunnel experiments on sand grains in the absence of clay and silt particles. We find only minor emissions of particulate matter from noncoated active sands under wind conditions typical of natural sand transport. The findings suggest that the dust generated by the mechanism of sand abrasion is less than dust generated by the removal of clay minerals coated on sand grain surfaces; both mechanisms on active sands produce far less dust than nonsandy soils. Feldspar sand was found to be slightly more effective at generating dust through abrasion than quartz sand. However, due to the low spatial coverage of feldspar sands in active sands worldwide, dust generated from feldspar abrasion may produce a relatively small contribution to global dust emissions. We thus conclude that sand abrasion by wind transport has a low potential to generate dust-sized particles from active sands.

1. Introduction

Mineral dust emission is a major phenomenon influencing many aspects of the Earth system. Dust aerosols affect Earth's global energy balance and climate sensitivity through radiative effects and climate feedbacks (e.g., Kok et al., 2018) and cloud-formation processes, especially for ice and mixed-phase clouds (DeMott et al., 2015; Nenes et al., 2014). Dust storms also influence nutrient cycling on terrestrial and marine ecosystems (e.g., Jickells et al., 2005; Katra et al., 2016) and are considered a key air pollutant producing substantial health risks (Giannadaki et al., 2014; Vodonos et al., 2015).

Past studies have simulated the global cycle of mineral dust (Albani et al., 2014; Ginoux et al., 2004; Ginoux et al., 2001; Huneeus et al., 2012; Klose & Shao, 2013; Knippertz & Todd, 2012; Kok et al., 2014). The annual global dust emissions are estimated to be as high as 3×10^9 tons (Huneeus et al., 2011; Kok et al., 2017). However, comparisons of model results against dust measurements still show large discrepancies (Evan et al., 2015; Kok et al., 2017). These gaps are due to a variety of factors, mainly uncertainties in the surface properties incorporated into models and identification of dust sources. Most models have used dust emission schemes that assume dust is mainly emitted from nonsandy soils containing a large fraction of very fine materials—clay and fine silt-sized particles (Paul Ginoux et al., 2001; Zender et al., 2003). However, recent measurement studies have found a significant contribution of active sands (e.g., dunes and sand sheets) to dust emissions in Northern Africa, China, and elsewhere (Crouvi et al., 2012; Sweeney et al., 2016). This suggests that active sand bodies can generate major dust events on a global scale.

Active sand bodies such as dunes are soils containing more than 90% by mass of unstabilized (loose) sand-sized particles (80–1,000 μm in diameter) that are available for aeolian (wind-driven) saltation transport. These active sands cover around 20% of arid areas worldwide (Pye & Tsoar, 2009) and are also a dominant formation covering large areas of Mars, Venus, Titan, and Pluto (Charnay et al., 2015; Claudin & Andreotti, 2006). Most sand bodies on Earth consist of high percentages of quartz mineral (SiO_2) (Nesbitt

& Young, 1984; Pye & Tsoar, 2009). The second most dominant mineral of sand grains is feldspar with a dominance of alkali feldspars (Na_x-$K_{1-x}AlSi_3O_8$). Feldspar is not likely to appear alone in sand dunes but rather as a mixture with other minerals, usually with quartz (Muhs, 2004). Quartz has relatively high hardness level of 7.0 on Mohs scale (logarithmic scale of mineral hardness), compared with 6.0 for feldspar, as a result of different mineralogical structures (Broz et al., 2006). This gives the quartz mineral the ability to resist weathering over time (Wayne Nesbitt et al., 1997). Thus, in nature, most continental (inland) sand bodies formed by distal sources contain mainly quartz sand grains (Muhs, 2004). Understanding the role of active sand in dust emission processes is essential to properly quantify and simulate global dust in regional and global models.

Studies on dust emission from active sand in drylands have proposed sand abrasion by wind transport (aeolian abrasion) as the main mechanism for dust generation (Bhattachan et al., 2012; Bullard et al., 2004; Crouvi et al., 2012; Sweeney et al., 2016; Wright et al., 1998). Aeolian abrasion refers to the mechanical wear and fracture of sand grains due to the impacts of saltators at the sand bed or by sand collisions in the air (Kuenen, 1960). Aeolian abrasion results in the formation of finer dust particles, including clay (<2 μm in diameter) and silt (between 2 and 63 μm in diameter) sized dust particles. Some previous studies have referred to the removal of minerals that coat on the surface of the sand grains as a form of aeolian abrasion (Bullard et al., 2004, 2007). However, here we only focus on the basic mechanism of aeolian abrasion, that is, the reductions in the physical size and angularity of parent sand grains (Bagnold, 1937; Jerolmack et al., 2011; Jerolmack & Brzinski, 2010; Kuenen, 1960). The rate of aeolian abrasion appears to be controlled by the dynamics of sand collisions, which depends on the grain size, shape, mineralogy, and wind properties (Bhattachan et al., 2012; Wright et al., 1998). For instance, positive relationships between abrasion rates and particle size and angularity were found (Kuenen, 1960).

However, all the abovementioned studies have been carried out in artificial conditions of glass "test-tube" chambers that do not simulate natural aeolian processes of saltating sand particles (Bullard et al., 2004, 2007; Kuenen, 1960; Smith et al., 1991; Whalley et al., 1982, 1987; Wright et al., 1998). Recent aeolian simulations in a boundary layer wind tunnel and field measurements have suggested that aeolian abrasion produces only a minor contribution to dust generation from active sands (Huang et al., 2019; Swet et al., 2019). Both studies show that the removal of clay coatings from the surface of quartz and feldspar sands is a dominant mechanism of dust emission. The sand coatings are very fine layers of mainly iron and clay-rich minerals present on the surfaces of sand grains. These coatings were found to be released as very fine dust particles (PM_{10} and $PM_{2.5}$ emissions) from active sands by mechanical weathering in the laboratory chamber (Bullard et al., 2007; Bullard & White, 2005) and by saltation transport in the field (Huang et al., 2019) and the wind tunnel (Swet et al., 2019). However, the assumption that aeolian abrasion is the dominant mechanism of dust emission from active sands is still the prevailing argument in the literature (Bhattachan et al., 2012; Bullard et al., 2004; Crouvi et al., 2012; Sweeney et al., 2016; Wright et al., 1998). Moreover, the theory of sand abrasion is used to explain the formation of finer soils (loess) at the leeward side of dune fields by deposition and accumulation of silt-sized particles (2–63 μm) (Crouvi et al., 2008; Smith et al., 1991; Whalley et al., 1982). However, the observed spatial fining trends may also result from sorting or fractionation caused by differences in transportability of different grain sizes (Roskin et al., 2014). Dust generation (rates and products) by sand abrasion has never been tested under saltation conditions, and the question of the relative contribution of this mechanism to dust generation from sands to the global dust cycle is still unsolved.

To fill this clear research gap, we explore dust emission by sand abrasion in targeted simulations of aeolian sand transport (saltation). Our study combines wind tunnel experiments and sample analyses of noncoated quartz and feldspar sands. Understanding the dust emission mechanism from active sand can provide more accurate estimates of quantities and particle characteristics of global dust loading to the atmosphere, thereby reducing uncertainties in chemical transport and global climate models. It can also advance our understanding of sand transport and landscape development on both the Earth and other planets, like Mars.

2. Materials and Methods

In order to measure the dust emission potential from active sand in response to the abrasion mechanism, we performed wind tunnel experiments to simulate the conditions of saltation transport. During the experiments, sand samples were collected to measure changes in particle size distribution (PSD) and

morphology by using Scanning Electron Microscope (SEM) analyses. The wind tunnel experiments and sand analyses were performed on clean (noncoated) quartz sand and feldspar-quartz sand, respectively.

2.1. Sand Samples

For the experiment, we have used two noncoated sand samples to quantify the aeolian abrasion of active sands. Quartz sand and feldspar-quartz sand were chosen for the experiments to represent the most dominant minerals in natural active sands. We used clean sands (no clay coatings and no residence fines) in order to control variables and focus only on aeolian abrasion.

Quartz is the most abundant sand-forming mineral on Earth, especially in inland dune fields (Pye & Tsoar, 2009). We used quartz sand (sand [50–70 mesh], Sigma-Aldrich, cat 274739, Lot MKCC7972- USA) with no coatings and no loose dust-size particles in-between the sand grains, which instead exist in natural dune sands (Swet et al., 2019). The quartz sand consists of subangular grains (R of between 0.27 and 0.33), according to Powers (1953) roundness classification. PSD analysis shows a range of 150–600 μm and a mode of 350 μm in diameter. The quartz sand contains 100% SiO_2 minerals (including 96.4% Quartz and 3.6% Coesite) by chemical and mineralogical analyses using X-ray power Fluorescence (XRF) and X-Ray Diffraction (XRD). The quartz sand samples contain no surface coatings, confirmed by scanning transmission electron microscope (STEM) images (Figure 1), and XRD analysis, showing no other material beside SiO_2. The analysis was conducted on 20 random-selected samples (hundreds of particles in each sample).

For comparison, feldspar-quartz sand that contains ~50% by mass quartz and ~50% alkali feldspars was also tested in this study. The feldspar-quartz sand was collected from the Oceano dunefield in California, which was formed by strong onshore sea breezes transporting sand derived from fluvial deposits (Cooper, 1967). The feldspar-quartz sand is composed of relatively coarse sand particles (mode ~400 μm in diameter) with a low amount (<1%) of dust-sized particles (Huang et al., 2019; Swet et al., 2019). Sand samples from this site were taken from the upper 2-cm layer of the dunes crest. Before the aeolian experiments, the feldspar-quartz sand first went through a washing and drying process to remove loose and attached dust-sized particles (Swet et al., 2019). Second, the feldspar-quartz sand was saturated in a sodium carbonate solution (Na_2Ca_3) in a concentration of 0.05% for 12 hr to ensure the removal of the attached clay coatings. Finally, the sand was washed with water and dried again before entry into the wind tunnel. After the above processes, the feldspar-quartz sands contain no surface coatings, confirmed by STEM images (Figure 1c) and XRD mineral composition analysis.

Note that both the quartz sand and feldspar-quartz sand used in this study are somewhat coarser (mode of 350–400 μm in diameter) than typical aeolian sand dunes worldwide (mode of 125–250 μm in diameter; Pye & Tsoar, 1990). In addition, the particle shapes of the quartz sand and feldspar-quartz sand are both characterized as subangular (R of between 0.28–0.33 and 0.25–0.30, respectively), compared to the subrounded sand typical for inland sand dunes (Goudie & Watson, 1981). These size and shape parameters make the sand used in this study more susceptible to aeolian abrasion than typical aeolian sand. That is, angular sand grains can allow a better examination of the mechanical wear and rounding of the grains over time to produce dust-sized particles (Bullard et al., 2007; Gillette, 1978; Khalaf & Gharib, 1985; Kuenen, 1960; Whalley et al., 1982, 1987; Wright et al., 1998), while the coarser size of the grains ensures impacts with higher kinetic energy during saltation transport (Katra et al., 2014). Detailed description of the sand properties measuring methods are presented below.

2.2. Wind Tunnel Experiments

The aeolian experiments were performed using an open circuit wind tunnel consisting of three parts: an entrance cone, a test section, and a diffuser (Katra et al., 2014). The cross-sectional area of the tunnel is ~0.7 × 0.7 m, and the working length is 7 m for measurements in the test section (see supplementary Figure S2 in Swet et al., 2019). The boundary layer in the wind tunnel is ~22 cm above the tunnel bed (Katra et al., 2014). Instruments installed in the wind tunnel enable the determination of the following parameters: (i) wind velocity in vertical and horizontal cross sections by microvane probes (www.kimo.com) for calculation of shear velocity (u_*, in m s^{-1}) through the *law of the wall* 1:

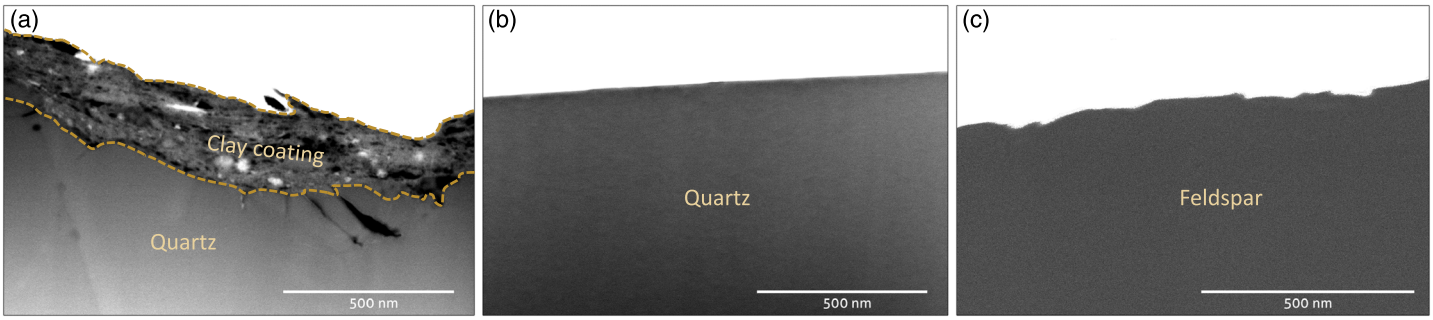

Figure 1. Differences in sand grain profile between coated and noncoated sand. Profile STEM 3+ (scanning transmission electron microscope) images of sand grains cut and processed in a dual-beam SEM/FIB device. (a) Typical quartz sand dune grain (SiO_2) covered with ~200-nm clay coating layer (bordered on both sides by a yellow line). The sand was collected from an active sand dune from the Negev dunefield, which is located in the eastern part of the Sinai-Negev erg. (b) Quartz sand (SiO_2) with no coatings attached to the surface of the grain purchased from Sigma-Aldrich. (c) Feldspar sand grain ($KAlSi_3O_8$) with no coatings attached to the surface of the grain.

$$\frac{u}{u_*} = \frac{1}{K} \ln \frac{z}{z_0}, \tag{1}$$

where u_* is the wind shear velocity (m s^{-1}), u is the wind velocity (m s^{-1}) at a specific height z (m), z_0 is the aerodynamic roughness length of the surface (in m), and K is von Karman's constant (≈ 0.4).

The wind profile was measured at different heights above the tunnel bed: 2, 3.5, 5, 7.5, 10, 15, 20, 25, 30, 35, 40, and 45 cm; (ii) collection of saltating sand grains by a vertical array of traps oriented along the wind direction for calculating the vertical-integrated horizontal saltation mass flux (kg m^{-1} s^{-1}) over time. The traps were placed at heights of 2.5, 4.5, 6.5, 8.5, and 10.5 cm above the tunnel bed, and each trap had a cross section of 2×1 cm. The sand was collected and weighted separately every 10 min, (iii) dust concentrations (mg m^{-3}) of particles that are less than 10 μm in aerodynamic diameter (PM_{10}), recorded by a light-scattering device, DustTrak DRX 8534 (ww.tsi.com), in the range of 0.001–150 mg m^{-3} (manufacturer stated error is ±0.1% of reading) at 1-s intervals, placed at 20 cm above the tunnel bed, which is above the saltation layer but within the boundary layer. Production of coarser dust-sized particles (10–63 μm) via abrasion was analyzed by PSD of the sand grains following the experiments.

In each experiment, the sand was placed in an ~3-cm-thick layer on the full length of the wind tunnel bed. The experiment was conducted under a shear velocity of 0.36 m s^{-1} (corresponding to a free stream wind velocity of 7.9 m s^{-1}, measured at 25 cm above the tunnel bed), which caused sand grains to enter saltation transport with no suspension of sand-sized particles. The time duration of each experiment was up to 14,400 s (240 min). In this time duration, the sand was manually recycled and stirred in the tunnel, thereby the majority of the grains was exposed to the wind in the tunnel and thus to the saltation transport. Based on the tunnel dimensions, the amount of saltators collected by all five traps during each experiment, and the initial amount of sand inserted into the wind tunnel for the experiment, we calculated that a single sand grain traveled four times of the tunnel length on average (4×7 m = ~30 m). Note that the experimental setup provides a much longer time period of sand exposure to specific wind (i.e., 0.36 m s^{-1}) than would typically be sustained in the field (Comola et al., 2019). The saltation flux remained constant (within ±10%) during the experiment and did not fade or intensify over time (Katra et al., 2014; Schmerler et al., 2016). Each run (14,400 s, ~30 m) was repeated three times to determine the mean values and errors of saltation flux and dust emission for each of the two sand samples.

Before each experiment, the PM_{10} background levels were measured inside the tunnel to account for noise in the measured PM_{10} signal. The noise that came from nondust aerosols, electronic noise, and atmospheric dust measured inside the laboratory/tunnel in the day of the experiment is on average around 0.027 mg m^{-3}. The background values measured in the DustTrak were compared for data verification with HAZ-DUST EPAM-5000 device installed inside the wind tunnel. In addition, the background data are consistent with previous studies that examined the background values in the city of Be'er Sheva (where the wind tunnel is located) and showed a good fit between the data of the DustTrak and the gold-standard instrument of TEOM™ Continuous Ambient Particulate Monitor (Krasnov et al., 2015).

The recorded PM_{10} concentrations (mg m^{-3}) and sand fluxes (kg m^{-1} s^{-1}) were used to calculate the sandblasting efficiency (m^{-1}). Sandblasting efficiency is the vertical dust flux produced by a unit horizontal sand saltation flux and, therefore, is an important property to inform the dust emission mechbanism (Kok et al., 2014; Martin & Kok, 2018). We first converted the PM_{10} concentrations into the mass flux emitted from the sand surface (F_{PM}, in kg m^{-2} s^{-1}) based on the wind tunnel dimensions and wind velocity:

$$F_{PM} = \left(C_{PM} - C_{bg}\right) \times V_{air} \times A_{cs}/A_p, \tag{2}$$

where C_{PM} is the recorded PM_{10} concentrations (kg m^{-3}) from the sand, C_{bg} is the averaged PM_{10} background concentration (kg m^{-3}) over the time duration of the experiment, V_{air} is the mean horizontal wind velocity (averaged over height) in the boundary layer (7.2 m s^{-1}), A_{cs} is the cross section of the boundary layer in the wind tunnel (0.154 m^2), and A_p is the area of the experimental plot (4.9 m^2). We then used the PM_{10} flux (kg m^{-2} s^{-1}) to calculate the sandblasting efficiency α (m^{-1}) (Kok et al., 2014):

$$\alpha = F_{PM}/Q, \tag{3}$$

where Q (kg m^{-1} s^{-1}) is the total horizontal sand flux integrated over the entire experiment time for all sand grain sizes (calculated from the sand traps). That is, the sandblasting efficiency quantifies PM_{10} dust generation per unit of sand flux produced by all sizes of saltators. See Table S1 for more details.

2.3. Particle Analyses

Physical and chemical properties of the sands (before and after the aeolian experiments) were analyzed in the laboratory. Particle size, morphology, mineralogy, and chemistry of unprocessed sands before the aeolian experiments were analyzed. In addition, processed sands from the tunnel bed and the sand traps were analyzed after each run to quantify the changes in particle size and morphology following the saltation collisions.

The PSDs of the unprocessed sand samples and the changes in the size of sand grains during the experiments were analyzed by the laser diffractometer method using the Mastersizer 2000 (Malvern Instruments, Malvern, UK). The Mastersizer 2000 uses a 90 detector array and measures particles in the size range of 0.02–2,000 μm. PSD data were calculated using the Lorenz-Mie scattering theory using a particle refractive index and particle absorption index of, respectively, 1.54 and 0.003 that fit both sands since the feldspar-quartz sand contains a mixture of both minerals (Bohren & Huffman, 1983). The Malvern proprietary software (Version 5.6) was employed to determine the mean diameters, median diameters, and size fraction weights of 10%, 50%, and 90% of the sample ($d(0.1)$, $d(0.5)$, and $d(0.9)$, respectively).

The mineralogical composition of the unprocessed sand was analyzed using the X-ray power diffraction method (Philips 1050/70 power diffractometer). A Panalytical Empyrean Powder Diffractometer equipped with position sensitive detector X'Celerator was used. Data were collected in the q/2q geometry using Cu K_α radiation ($\lambda = 1.54178$ Å) at 40 kV and 30 mA. Scans were run during ~15 min in a 2θ range of 4–60° with step equal to ~0.033°. Elemental composition analyses were performed by the XRF method using an XRF spectrometer PANalytical Co., model Axios (wavelength dispersive -WDXRF, 1 kW). The Omnian software was used for the quantitative analysis.

Morphological and chemical characteristics of both unprocessed and processed sand grains were examined using a SEM (Quanta 200, FEI). The high magnification (6X to >1,000,000X) enabled the analysis of the smallest dust particles (<2 μm). Energy dispersive spectroscopy sensor was used for chemical compositional information. Sand-grain roundness was calculated from imaged grains by manually inscribing circles on each sand grain. Roundness (R) was defined as the ratio of the radius of curvature of surface features, r_i, to the radius of the largest inscribed circle, r_{max}, yielding the size relation (Rousé et al., 2008; Wadell, 1932). The R values were compared with the Powers (1953) classification chart for roundness level: very angular ($0.12 < R < 0.17$), angular ($0.17 < R < 0.25$), subangular ($0.25 < R < 0.35$), subrounded ($0.35 < R < 0.49$), rounded ($0.49 < R < 0.7$), and well rounded ($0.70 < R < 1.00$).

The surface coatings of sand grains and their morphological and chemical characteristics were examined using a DualBeam Microscope (Helios G4 UC, Thermoscientific), which incorporates both a focused ion beam and a SEM in a single system. In order to allow conductivity, a thin layer (8 nm) of gold (Au) was

obtained to coat the top of the sand grains. In order to create a vertical profile of sand grains, a thin slice ($10 \times 5 \times 0.01$ μm) model was carved from the sand surface using the focused ion beam. To protect against contamination of the surface by the ions of the carving area was first coated by a layer of platinum (Pt). Structural information of the sand grain surface was analyzed by STEM images. Also here, energy dispersive spectroscopy was used for chemical compositional information.

3. Results and Discussion

3.1. Dust Emission From Noncoated Sand Under Saltation

Under saltation transport simulated in the wind tunnel, we measured the particulate matter (PM) emission from pure quartz sands and feldspar-quartz sands with no coatings attached to their surfaces (Figure 1). The lack of coatings enabled us to isolate the effect of aeolian abrasion for better exploration of the dust emission mechanism rate and product.

The results of the noncoated sand show only minor PM_{10} emissions under a common shear velocity ($u_* = 0.36$ m s^{-1}) and saltation transport (Figures 2 and 3). The PM_{10} concentrations produced by the quartz sand show a relatively weak trend over time, ranging from 0.024 to 0.043 mg m^{-3}, with an average PM_{10} concentration of only 0.033 mg m^{-3} (Figure 2a and Table S1). The PM_{10} emissions recorded from the quartz sand are very close to the measured background levels (average of 0.027 mg m^{-3}; black line in Figure 2) during the whole experiment duration. The PM_{10} trend is consistent with the steady saltation recorded during the quartz sand experiment (Figure 3). The saltation fluxes in this study matches the results received in previous studies on active sand transport for the same shear velocity of 0.36 m s^{-1} (Katra et al., 2014; Schmerler et al., 2016; Swet et al., 2019). However, the wind tunnel experiment on the feldspar-quartz sand showed a pattern of slight decrease in PM_{10} concentrations over time toward very low values after ~170 min (Figure 2b). The saltation fluxes from the feldspar-quartz sand also remained relatively stable throughout the experiment with flux around 2.5×10^{-3} kg m^{-1} s^{-1} (Figure 3) and in accordance with previous wind tunnel and in situ experiments on feldspar-quartz sand (see Table 1 in Martin & Kok, 2018; Swet et al., 2019, respectively). The lower saltation flux in the feldspar-quartz sand compared to the quartz sand is most likely due to its coarser PSD (see section 2), because the threshold shear velocity is required to sustain saltation increases with the grain particle size (Kok et al., 2012).

The PM_{10} fluxes produced by both quartz (average over time of 1.5 μg m^{-2} s^{-1}) and feldspar-quartz (average over time of 2.3 μg m^{-2} s^{-1}) sands in this study are much lower than those obtained in other studies on active sand dunes. Previous laboratory experiments on the sand abrasion mechanism have showed higher dust-sized particle generation from sand grains (Smith et al., 1991; Sweeney et al., 2016; Whalley et al., 1982, 1987; Wright et al., 1998). However, these studies did not test the dust generation under saltation process. Sweeney et al. (2016), for example, recorded PM_{10} fluxes of over 500 μg m^{-2} s^{-1} from coated sand dunes using a PI-SWERL. Huang et al. (2019) and Swet et al. (2019) recorded PM_{10} fluxes of up to ~50 μg m^{-2} s^{-1} under saltation but from coated sand. Figure 4 provides a visual comparison between the PM_{10} fluxes (μg m^{-2} s^{-1}) emitted from the noncoated sand from this study and of previous wind tunnel experiments on coated sands and nonsandy dust sources. The dust emission rates from the noncoated sand are very low compared to both coated sands and nonsandy soil. The dust emissions of the typical (coated) quartz active sand dunes, containing 98% of sand-sized grains, from the wind tunnel experiment, were mainly due to the removal of clay coatings (Swet et al., 2019). Although under similar conditions of grain sizes, wind shear velocity, and saltation flux, the dust emissions are considerably lower in the absence of clay coatings on the sand grains surface (Figure 4). The PM_{10} fluxes produced by the nonsandy soils are higher by about 3 orders of magnitude than PM_{10} fluxes produced by coated sands and more than 4 orders of magnitude higher than fluxes produced by noncoated sand (Figure 4). It should be noted that the example of the nonsandy (loess) soil presented in Figure 4 is common to aggregated topsoil, where for disturbed topsoil, the PM_{10} rates may reach much higher levels.

3.2. Sandblasting Efficiency From Quartz and Feldspar Sand Grains

The calculated bulk sandblasting efficiency (m^{-1}) provides a further insight into the dust PM generation ability of the sand (Figure 5). The sandblasting efficiency is the ratio between the vertical dust emission flux (kg m^{-2} s^{-1}) and the horizontal sand saltation flux (kg m^{-1} s^{-1}) (Kok et al., 2014; Martin & Kok, 2018). The

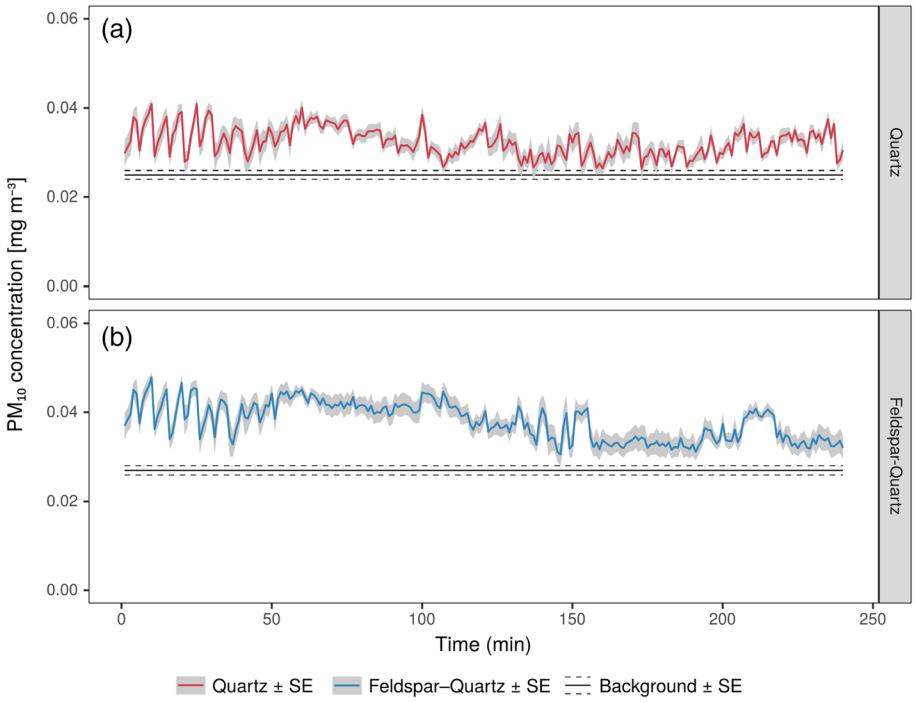

Figure 2. PM_{10} concentrations measured during the wind tunnel experiments. Average PM_{10} concentrations in mg m^{-3}, of the three experimental runs, of the quartz sand (a) and feldspar-quartz sand (b). The black lines represent the average background levels ± the standard error (dashed lines). The background levels were measured before and after each experiment run. It should be noted that the background levels (average of 0.027 mg m^{-3}) were not subtracted from the PM_{10} results of the sands. In order to reduce measurement noise, the PM_{10} concentrations presented here are an average over time intervals of 60 s. The PM concentrations and background concentrations of each run are presented in Table S1.

average sandblasting efficiency of the clean quartz sand was found to be lower than the value reported for typical coated quartz sand dunes and the range of 10^{-2} to 10^{-5} m^{-1} reported for nonsandy soils (Figure 5). These results emphasize the low ability of the noncoated sand to generate dust through saltation transport. Under the same shear velocity of 0.36 m s^{-1}, coated quartz sand received sandblasting

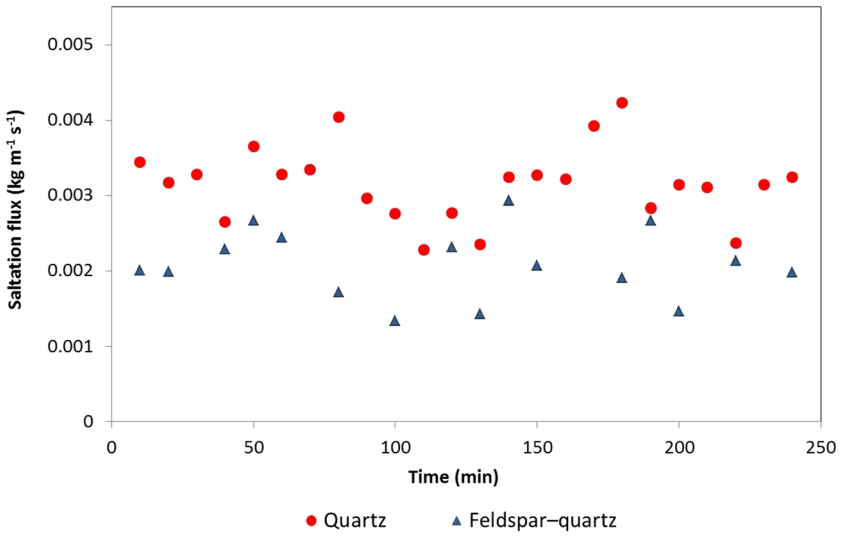

Figure 3. Saltation fluxes measured during the wind tunnel experiments. Saltation fluxes (in kg m^{-1} s^{-1}) of the clean quartz sand (red) and feldspar-quartz sand (blue). The fluxes presented here are an average of the three experimental runs. Note that eight saltation measurements of the feldspar-quartz were removed from the analysis due to technical problem during the experiment.

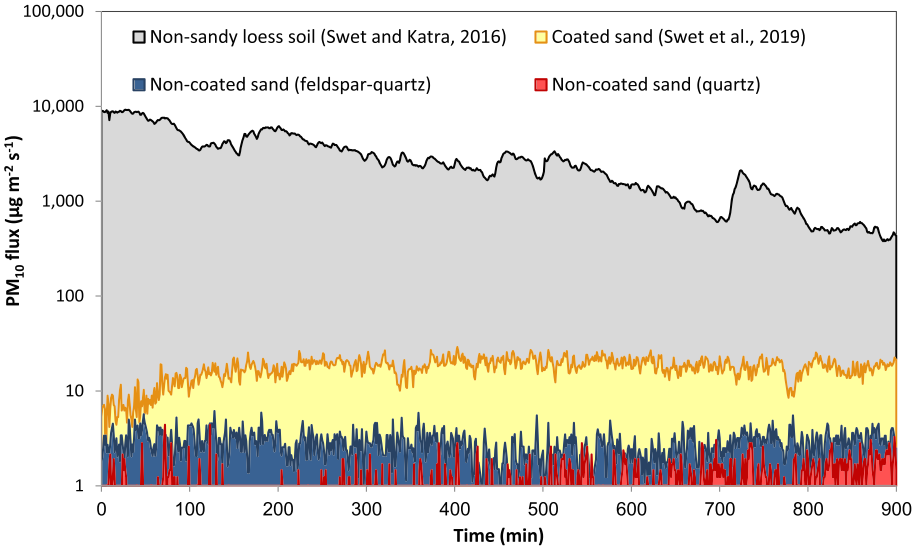

Figure 4. Comparison of dust emission rates between different dust sources. PM_{10} fluxes (μg m^{-2} s^{-1}) of quartz sand (red) and feldspar-quartz sand (blue). In addition, the chart shows the PM_{10} fluxes from previously published studies on active (coated) sand (Swet et al., 2019) and aggregated loess soil (Swet & Katra, 2016). All of the experiments were conducted in wind tunnels under wind velocity of ~7.5 m s^{-1} (measured 20 cm above the tunnel bed), and the PM_{10} fluxes were calculated based on Equation 1. Note the logarithmic scale in *Y* axis.

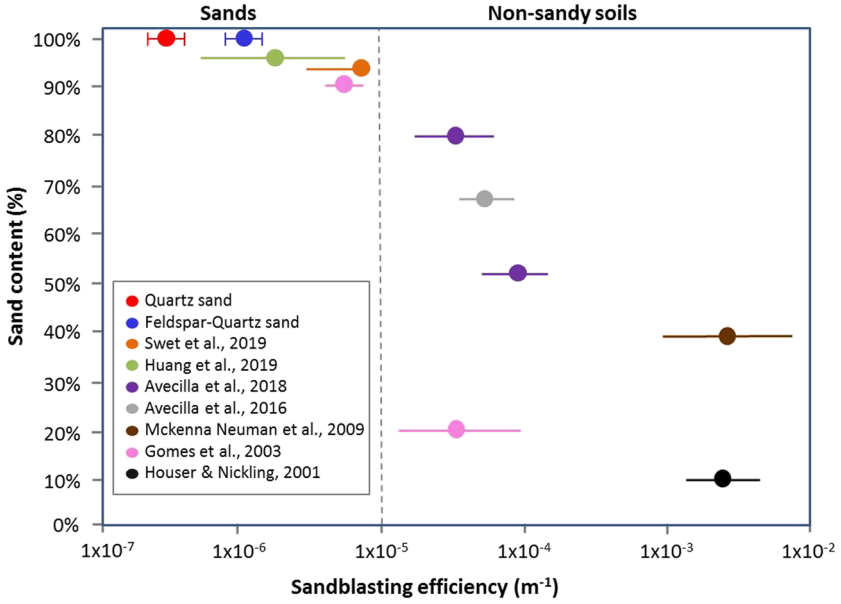

Figure 5. Sandblasting efficiency comparison to previously published studies on coated-sand and nonsandy soils. Calculated averaged sandblasting efficiency (m^{-1}) of the clean quartz sand (red) and feldspar-quartz sand (blue) ± the standard error in bars, measured under shear velocity of 0.36 m s^{-1}. In addition, the chart shows the sandblasting efficiency of previously published studies of coated active sands (Gomes et al., 2003; Huang et al., 2019; Swet et al., 2019) and nonsandy soils (Avecilla et al., 2016, 2018; Gomes et al., 2003; Houser & Nickling, 2001; McKenna Neuman et al., 2009). The dot markers presented for these studies represent similar wind velocity conditions of this study. The horizontal uncertainty ranges that deviate from the markers represent different shear velocities. Note that Avecilla et al. (2018) and Gomes et al. (2003) present sandblasting efficiency of two soils containing different amounts of sand. The PM sandblasting efficiency calculations for each run of the quartz sand and the feldspar-quartz sand are presented in Table S1. The range within 10^{-5} to 10^{-2} m^{-1} envelopes the sandblasting efficiency of nonsandy soils (Gillette, 1978; Kok et al., 2012).

efficiency of 1.37×10^{-5} m^{-1} (Swet et al., 2019), compared to only 4.7×10^{-7} m^{-1} for the quartz sand that is more than an order of magnitude lower. Moreover, these findings are consistent with the assumption that the sandblasting efficiency increases sharply with the amount of fine nonquartz materials in the clay/silt size fraction (Katra et al., 2014; Kok et al., 2012). The lack of fine material in the quartz sand (99.6% sand-sized particles by mass) resulted in very low dust emission compared to typical dune quartz sands (orange in Figure 5), although the saltation flux remains similar (Swet et al., 2019).

The average sandblasting efficiency of the clean feldspar-quartz sand (blue in Figure 5) ranges between 9.4×10^{-7} and 3.2×10^{-6} m^{-1} with an average of 1.1×10^{-6} m^{-1}, which is much higher than for the clean (noncoated) quartz sand (red in Figure 5). The significantly higher sandblasting efficiency of the feldspar-quartz is in contrast with the small difference found in the PM_{10} concentrations of noncoated sands (Figure 2). Field experiments on coated feldspar-quartz sand (Huang et al., 2019) showed relatively low PM_{10} emissions compared to other nonsandy soils but a bit higher than those received from the noncoated feldspar-quartz sand in this study. The dust emission described for the coated feldspar-quartz sand is in general considered as low (Huang et al., 2019), and therefore, the impact of the coatings removal on the dust emission is probably small. Thus, the difference in the sandblasting efficiency between the coated feldspar-quartz sand (green in Figure 5) and the noncoated feldspar-quartz sand (blue in Figure 5) is relatively low.

3.3. Changes in Sand Size Due to Abrasion

It is generally assumed that the abrasion mechanism reduces the size of the saltating sand grains over time and increases the amount of fine particles in the sand over time (Bagnold, 1937; Kuenen, 1960). We assumed that PM_{10} and silt particles that may have been produced via saltation transport are emitted from the wind tunnel during the experiments. Since the PM_{10} was recorded during the experiments, the focus here was on the changes in the size distribution of the saltators that should indicate silt generation. Size and shape of the saltators were measured by PSD and SEM imagery structural analysis. The results of the PSD analyses show the difference in abrasion potential between the quartz and the feldspar minerals (Figure 6). The results of the quartz sand showed no significant difference (p value = 0.08 from Student's T test) in the PSD for all 90 size bins (Figure 6a). Figure 6b shows the change in $d(0.1)$, $d(0.5)$, and $d(0.9)$ parameters of the quartz sand over time relative to the first measurement (T1). There was no change in the particle size of the sand grains over time. A linear regression test examining the changes in the $d(0.1)$, $d(0.5)$, and $d(0.9)$ parameters over time shows no statistically significant trend linking the particle size to the time duration ($r^2 = 0.01$, p value = 0.66; $r^2 = 0.01$, p value = 0.62; and $r^2 = 0.02$, p value = 0.56, respectively).

On the other hand, the PSD analysis of the feldspar-quartz sand shows some differences in the PSD analysis between the samples over time (Figure 6c). However, a minor reduction in the grain size was found to be after 30 min and then a stable PSD over the rest of the experiment (Figure 6d). The regression analysis of the $d(0.1)$, $d(0.5)$, and $d(0.9)$ parameters over time show a stronger downward trend over time ($r^2 = 0.45$, p value = 0.01; $r^2 = 0.25$, p value = 0.09; and $r^2 = 0.36$, p value = 0.04, respectively) compared to the quartz sand. These results are compatible with the PM_{10} concentrations pattern of slight decrease over time found in the feldspar-quartz sand (Figure 2). It should be noted that the saltation fluxes from the feldspar-quartz remained relatively stable throughout the experiment around 2.5×10^{-3} kg m^{-1} s^{-1} (Figure 3).

We assume that the slight decrease in the grain size of the feldspar-quartz sand following saltation is related to abrasion of the feldspar particles. The feldspar mineral is considered to be weaker by an order of magnitude than quartz according to the Mohs hardness scale. It is chemically more complex with less symmetric structure than the quartz and thus considered to be less resistant to mechanical and chemical weathering (Muhs, 2004; Nesbitt & Young, 1984; Nesbitt et al., 1997).

No clear differences were found by the SEM imagery of the sand shape, size, and microstructure over time in both quartz and feldspar-quartz sands (Figure 7). Roundness measurements of the sand grains did not show significant differences in R value over time (Figure 7). We do take into account that there might have been very small-scale weathering on the sand grains that are not been able to detect. As such, further work is needed to determine the specific impact of sand collisions during natural saltation on the grain shape and microstructures.

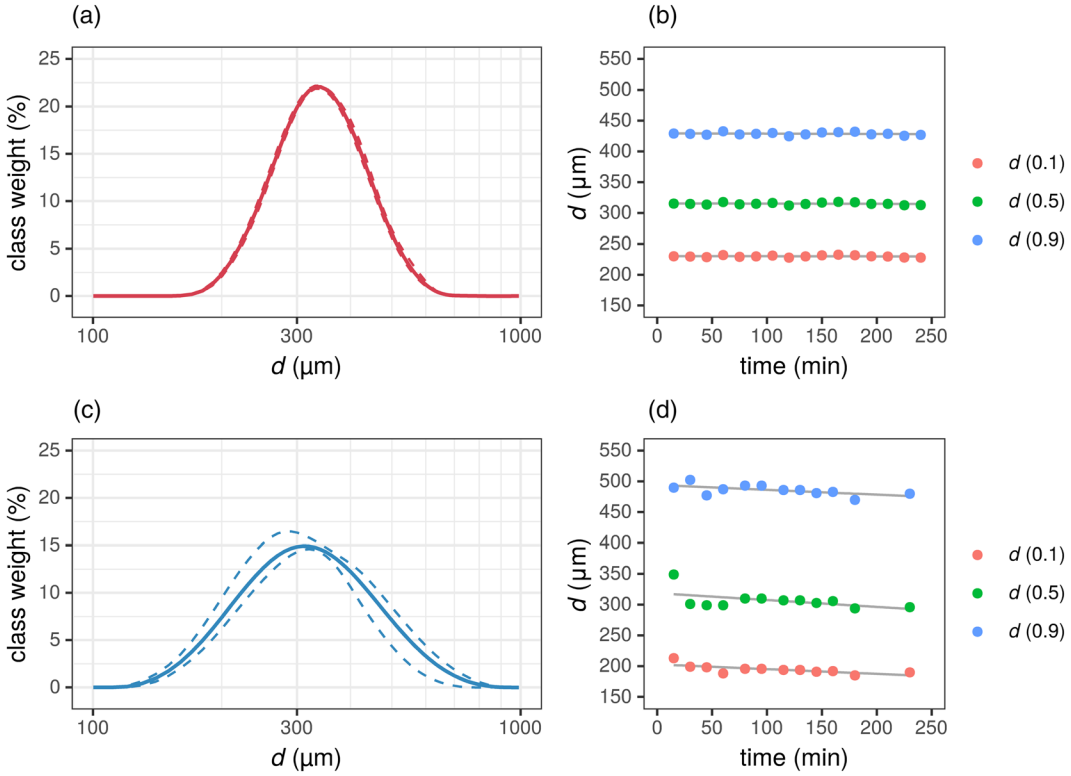

Figure 6. Particle size distribution (PSD) analysis over time of the quartz and feldspar-quartz sands saltating sand particles over the time period of the experiment (240 min). (a) and (c) represent the average PSD analysis (solid line) and the minimum and maximum PSDs over time (dashed lines) of the quartz sand and the feldspar-quartz sand, respectively. (b) and (d) show the change in the size fraction in which the PSD reaches 10%, 50%, and 90% (parameters of $d(0.1)$, $d(0.5)$, and $d(0.9)$) over time in the quartz sand and the feldspar-quartz sand, respectively. The PSD is of the saltating sand collected in the end of the wind tunnel. The solid gray lines in (b) and (d) represent the linear regression line of each parameter.

3.4. Dust Emission Potential From Aeolian Abrasion

The measurements of PM concentrations obtained in this study (Figure 2) provided further insight to the relative contribution of each of the dust emission mechanisms from active sands: (i) reemission of previously settled dust particles in the sand (Muhs et al., 2008), (ii) clay coating removal from sand grains (Bullard & White, 2005), and (iii) abrasion of the sand grains (Bhattachan et al., 2012; Bullard et al., 2007; Sweeney et al., 2016; Wright et al., 1998). To date, many studies have considered aeolian abrasion as the dominant mechanism for dust generation from active sands (Bhattachan et al., 2012; Bullard et al., 2004; Crouvi et al., 2012; Sweeney et al., 2016; Wright et al., 1998). However, according to the results presented above, the noncoated sand showed very low dust emission rates (Figure 2). Furthermore, Swet et al. (2019) suggested only minor contribution of aeolian abrasion to dust emission mechanisms from active sands. According to their results, the dominant mechanism for dust generation in typical active sand dunes is clay coating removal with small addition of dust reemission, depending on the initial content of loose dust particles between the sand grains. Yet, Swet et al. (2019) did not provide quantitative information on the specific role of aeolian abrasion in dust emission generation from active sands.

Figure 8 combines the results of this study with the dust emission mechanism analysis of Swet et al. (2019) for a better understanding of the role of the three dust generation mechanisms from active sands. It seems that the dominant dust emission mechanism from active sands is the removal of clay coatings (Bullard et al., 2007; Bullard & White, 2005; Huang et al., 2019; Swet et al., 2019) with some contribution of dust reemission (Swet et al., 2019) and only a minor contribution of aeolian abrasion. This provides, for the first time, quantitative information on the relative contribution of aeolian abrasion in dust generation during saltation of active sands. It should be noted that the results presented here are for typical quartz sand dunes, containing low amounts of loose fines between the sand grains (<2%), and may vary for sands with different extents of clay coatings and loose fines (Swet et al., 2019).

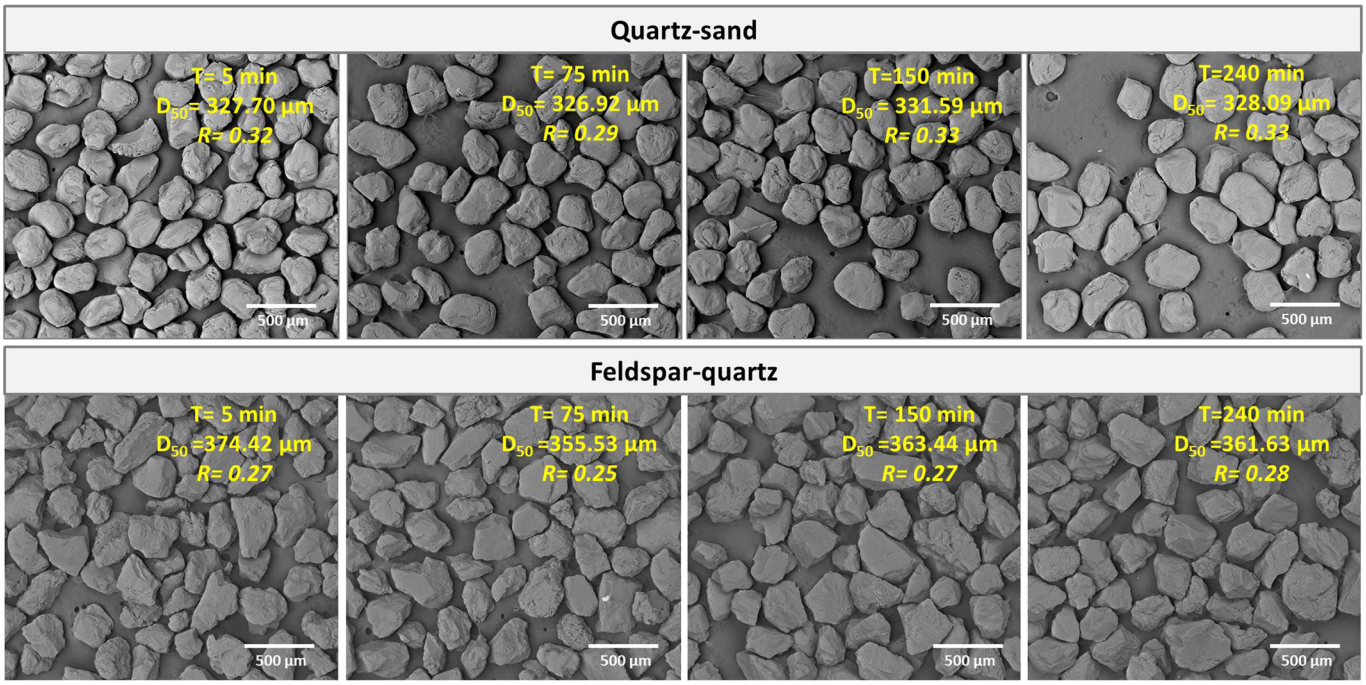

Figure 7. Scanning electron microscope images of sand samples collected from the quartz sand (top) and the feldspar-quartz sand (bottom) over the time duration of the wind tunnel experiment. T represent the time of the sand sampling after the beginning of the experiment, D_{50} represents the median size of all of the particles in each image, and *R* represent the average roundness value measured for each particle is the image.

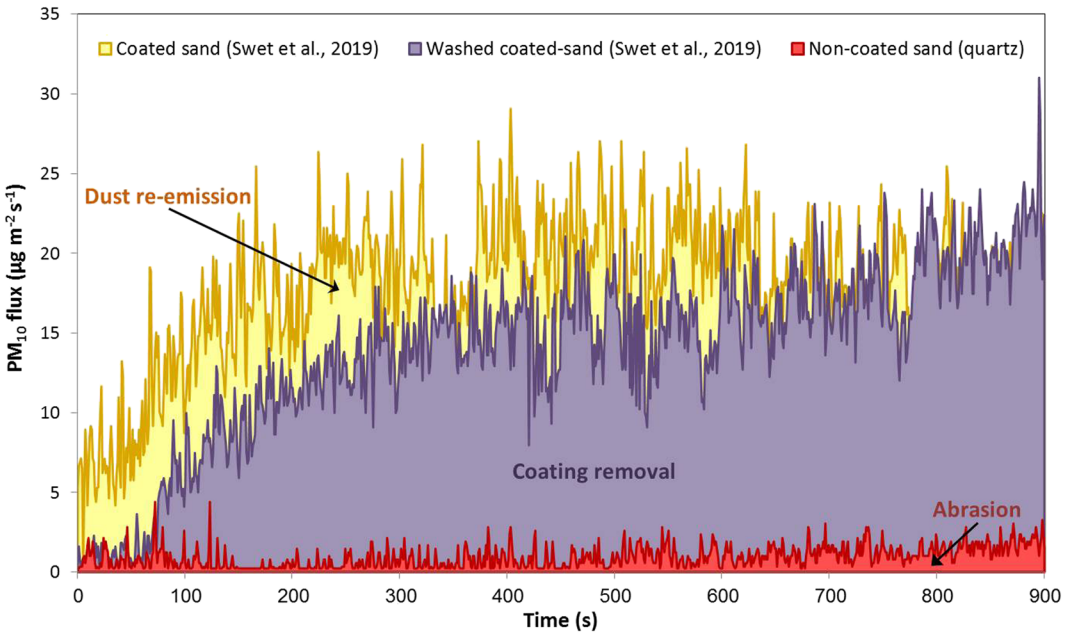

Figure 8. Dust generation potential of the three dust emission mechanisms from active quartz sand. The chart presents PM_{10} fluxes (µg m^{-2} s^{-1}) of noncoated quartz sand measured in this study (red) and coated quartz sand before (yellow) and after (purple) loose dust removal by washing and drying. The results of the coated sands are based on Figure 6 in Swet et al. (2019). All PM_{10} fluxes were measured under a shear velocity ($u*$) of 0.36 m s^{-1}. That is, the red line denotes dust generation by aeolian abrasion. The difference between the purple and red lines denotes dust generation by removal of clay-mineral coatings. The difference between the yellow and purple lines denotes dust reemission by settled loose dust.

3.5. Representativeness of our Results for Active Sands

It should be noted that the sand and dust fluxes in our wind tunnel experiments may differ from the natural settings. First, although the wind properties in the wind tunnel may differ somewhat from the complex behavior of natural wind (gusts, multidirectional flow), we believe that the aeolian experiment applied here is representative to the physical process of aeolian abrasion under saltation and provides information on show the relative contribution of the abrasion mechanism in dust emission from sands. Under this objective, we indeed find that the PM_{10} emission and sandblasting efficiency results obtained under the same experimental setup clearly show the difference in dust emission rates between the different dust sources (Figures 2 and 3). However, it should be taken into account that sandy areas can also include additional geomorphological units (e.g., playas, paleosol, and stabilized dunes), thus creating a certain spatial variability that may affect the quantification of dust emissions from the dune landscape. Second, the PSD of the two sand samples (with modes of 370 and 390 μm) can be coarser than that of other active sands worldwide. In most cases, sand dunes consist of sand grains with an average mode of ~200 μm (Pye & Tsoar, 2009). We consider that grains of different sizes can behave differently under the same wind shear velocity, although the quartz sand chosen for this study are medium-sized grains entering into saltation transport under common wind velocities. The impact energy of typical active sand dunes is expected to be lower than that of the sand used in this study (Thomas, 1987). In addition, typical inland sand dunes are characterized by more rounded sand grains than the subangular sand, which make the sand used in this study more susceptible to aeolian abrasion (Kuenen, 1960; Whalley et al., 1982, 1987; Wright et al., 1998). Thus, we can assume that the dust production through abrasion in typical sand dunes is even lower than of the results presented here. However, we acknowledge that more investigation can be done to explore the abrasion of sands in different sizes and shape and of sediments other than typical active sand.

Many coastal sands consist of relatively immature sediments that are characterized by course particles, higher angularity, and higher content of feldspar particles. These marine sediments were represented in this study by the feldspar-quartz sand from Oceano dunes. The PM_{10} concentration produced by the noncoated feldspar-quartz sand was higher than those emitted from the noncoated quartz sand (Figure 1). Still the sandblasting efficiency generated by the noncoated sands is substantially lower than that produced by other sandy (Huang et al., 2019; Sweeney et al., 2016) and nonsandy soils (Shao et al., 2011; Swet & Katra, 2016; Zobeck & Van Pelt, 2006). Third, in this study we found very low rate of PM_{10} (clay's and very-fine silt particles) generation, while emission of coarser dust-sized particles (10–63 μm) was not observed. PSD and SEM analyses of the satiating sand revealed no reduction in the actual size of the sand grains. Finally, the distribution of feldspar in sand bodies around the world is much lower than the feldspar-quartz sand in this study. The feldspar content in coastal dunes can go up to 50%, whereas continental dunes contain only ~5–15% feldspar (Anton, 1983; Lancaster et al., 2015; Muhs, 2004). Thus, when taking into consideration the small extent of the feldspar in sand fields around the globe, specifically in active sand dunes in arid zones, and the relatively low PM emissions, the contribution of the feldspar to the global dust emission by the abrasion mechanism may not be significant. Feldspar species are important as ice nuclei in cloud formation due to its high efficacy in freezing temperature (Welti et al., 2019). However, feldspar aerosols can be emitted into the atmosphere by nonsandy soils where this mineral is found in the size range of fine-silt and clays (<20 μm) that is produced in soils by hydro-chemical weathering processes (Nesbitt et al., 1997).

Under the four considerations above, our results of dust emission by aeolian abrasion are likely on the high end. Typical sand dunes worldwide can thus have an even smaller dust emission potential. The study results can be reprocess as empirical parameters in dust emission schemes (e.g., Kok et al., 2014). As such, further work is needed in determining the extent of dust generation from sands in global dust emission models, which assumed dust mainly emitted from nonsandy soils.

4. Conclusions

Active sand dunes have been proposed as significant contributors to the global dust cycle. Three main mechanisms are related to dust generation from active sands via saltation: reemission of previously settled dust particles in-between the sand grains, removal of clay coatings attached to the sand grains, and aeolian abrasion of saltating grains. The results of this study provide the first empirical results on dust generation produced by abrasion from noncoated saltating sand. We found only minor PM_{10} emissions from the

noncoated active sands under wind conditions typical of natural sand transport. The calculated sandblasting efficiency is much lower than that of coated sands, and both were substantially lower than the sandblasting efficiency of nonsandy soils. Our findings thus suggest only a low potential of dust generation from quartz active sand by abrasion. Although abrasion of feldspar sand was found to produce larger dust emission fluxes than for quartz sand, its low mass fraction in inland sand dunes reduces the contribution of feldspar abrasion to the global dust emission.

The results obtained in this study enable (i) a better understanding of the processes that generate dust from sands, where clay-coating removal is dominant mechanism rather than abrasion, with some contribution of dust reemission, and only a minor contribution of aeolian abrasion; (ii) a bottom-up assessment that dust emission from sand dunes is not likely to be an important component of the global dust cycle; and (iii) a parameterization of dust emission fluxes and sandblasting efficiency rates that can be implemented in future models. Further work is needed in determining the extent of dust generation from sands in global dust emission, which assumed dust mainly emitted from nonsandy soils.

Funding

The study was supported by a grant from the United States-Israel Binational Science Foundation (2014178) to I. K. and J. F. K.

Conflict of Interest

The authors declare that they have no competing interests.

Data Availability Statement

Data included in the analysis for this paper can be found on the Zenodo data repository (https://doi.org/10.5281/zenodo.3628542).

Acknowledgments
We would like to thank Dr. Michael Dorman for the help in result analysis and figure design.

References

Albani, S., Mahowald, N. M., Perry, A. T., Scanza, R. A., Zender, C. S., Heavens, N. G., et al. (2014). Improved dust representation in the Community Atmosphere Model. *Journal of Advances in Modeling Earth Systems*, *6*, 541–570. https://doi.org/10.1002/2013MS000279

Anton, D. (1983). Modern eolian deposits of the Eastern Province of Saudi Arabia. In M. E. Brookfield & T. S. Ahlbrandt (Eds.), *Developments in sedimentology* (Vol. 38, Pp. 365–378). Amsterdam Elsevier. https://doi.org/10.1016/S0070-4571(08)70805-7

Avecilla, F., Panebianco, J. E., & Buschiazzo, D. E. (2016). A wind-tunnel study on saltation and PM_{10} emission from agricultural soils. *Aeolian Research*, *22*, 73–83. https://doi.org/10.1016/j.aeolia.2016.06.003

Avecilla, F., Panebianco, J. E., Mendez, M. J., & Buschiazzo, D. E. (2018). PM_{10} emission efficiency for agricultural soils: Comparing a wind tunnel, a dust generator, and the open-air plot. *Aeolian Research*, *32*, 116–123. https://doi.org/10.1016/j.aeolia.2018.02.003

Bagnold, R. A. (1937). The transport of sand by wind. *The Geographical Journal*, *89*(5), 409. https://doi.org/10.2307/1786411

Bhattachan, A., D'Odorico, P., Baddock, M. C., Zobeck, T. M., Okin, G. S., & Cassar, N. (2012). The Southern Kalahari: A potential new dust source in the Southern Hemisphere? *Environmental Research Letters*, *7*(2), 024001. https://doi.org/10.1088/1748-9326/7/2/024001

Bohren, C. F., & Huffman, D. R. (1983). *Absorption and Scattering of Light by Small Particles*, New York: John Wiley & Sons, Inc.

Broz, M. E., Cook, R. F., & Whitney, D. L. (2006). Microhardness, toughness, and modulus of Mohs scale minerals. *American Mineralogist*, *91*(1), 135–142. https://doi.org/10.2138/am.2006.1844

Bullard, J. E., McTainsh, G. H., & Pudmenzky, C. (2004). Aeolian abrasion and modes of fine particle production from natural red dune sands: An experimental study. *Sedimentology*, *51*(5), 1103–1125. https://doi.org/10.1111/j.1365-3091.2004.00662.x

Bullard, J. E., Mctainsh, G. H., & Pudmenzky, C. (2007). Factors affecting the nature and rate of dust production from natural dune sands. *Sedimentology*, *54*(1), 169–182. https://doi.org/10.1111/j.1365-3091.2006.00827.x

Bullard, J. E., & White, K. (2005). Dust production and the release of iron oxides resulting from the aeolian abrasion of natural dune sands. *Earth Surface Processes and Landforms*, *30*(1), 95–106. https://doi.org/10.1002/esp.1148

Charnay, B., Barth, E., Rafkin, S., Narteau, C., Lebonnois, S., Rodriguez, S., et al. (2015). Methane storms as a driver of Titan's dune orientation. *Nature Geoscience*, *8*(5), 362–366. https://doi.org/10.1038/ngeo2406

Claudin, P., & Andreotti, B. (2006). A scaling law for aeolian dunes on Mars, Venus, Earth, and for subaqueous ripples. *Earth and Planetary Science Letters*, *252*(1-2), 30–44. https://doi.org/10.1016/j.epsl.2006.09.004

Comola, F., Kok, J. F., Chamecki, M., & Martin, R. L. (2019). The intermittency of wind-driven sand transport. *Geophysical Research Letters*, *46*, 13,430–13,440. https://doi.org/10.1029/2019GL085739

Cooper, W. S. (1967). *Coastal dunes of California* (Vol. 104). Geological Society of America. Retrieved from https://doi.org/10.1130/MEM104-p1

Crouvi, O., Amit, R., Enzel, Y., Porat, N., & Sandler, A. (2008). Sand dunes as a major proximal dust source for late Pleistocene loess in the Negev Desert, Israel. *Quaternary Research*, *70*(2), 275–282. https://doi.org/10.1016/j.yqres.2008.04.011

Crouvi, O., Schepanski, K., Amit, R., Gillespie, A. R., & Enzel, Y. (2012). Multiple dust sources in the Sahara Desert: The importance of sand dunes. *Geophysical Research Letters*, *39*, L13401. https://doi.org/10.1029/2012GL052145

DeMott, P. J., Prenni, A. J., McMeeking, G. R., Sullivan, R. C., Petters, M. D., Tobo, Y., et al. (2015). Integrating laboratory and field data to quantify the immersion freezing ice nucleation activity of mineral dust particles. *Atmospheric Chemistry and Physics*, *15*(1), 393–409. https://doi.org/10.5194/acp-15-393-2015

Evan, A. T., Flamant, C., Fiedler, S., & Doherty, O. (2015). An analysis of aeolian dust in climate models. *Geophysical Research Letters*, 5996–6001. https://doi.org/10.1002/2014GL060545@10.1002/(ISSN)1944-8007.GRLCMIP5

Giannadaki, D., Pozzer, A., & Lelieveld, J. (2014). Modeled global effects of airborne desert dust on air quality and premature mortality. *Atmospheric Chemistry and Physics; Katlenburg-Lindau*, *14*(2), 957–968. https://doi.org/10.5194/acp-14-957-2014

Gillette, D. (1978). A wind tunnel simulation of the erosion of soil: Effect of soil texture, sandblasting, wind speed, and soil consolidation on dust production. *Atmospheric Environment (1967)*, *12*(8), 1735–1743. https://doi.org/10.1016/0004-6981(78)90322-0

Ginoux, P., Prospero, J. M., Torres, O., & Chin, M. (2004). Long-term simulation of global dust distribution with the GOCART model: Correlation with North Atlantic Oscillation. *Environmental Modelling & Software*, *19*(2), 113–128. https://doi.org/10.1016/S1364-8152(03)00114-2

Ginoux, P., Chin, M., Tegen, I., Prospero, J. M., Holben, B., Dubovik, O., & Lin, S.-J. (2001). Sources and distributions of dust aerosols simulated with the GOCART model. *Journal of Geophysical Research*, *106*(D17), 20,255–20,273. https://doi.org/10.1029/2000JD000053

Gomes, L., Rajot, J. L., Alfaro, S. C., & Gaudichet, A. (2003). Validation of a dust production model from measurements performed in semi-arid agricultural areas of Spain and Niger. *Catena*, *52*(3-4), 257–271. https://doi.org/10.1016/S0341-8162(03)00017-1

Goudie, A. S., & Watson, A. (1981). The shape of desert sand dune grains. *Journal of Arid Environments*, *4*(3), 185–190. https://doi.org/10.1016/S0140-1963(18)31559-3

Houser, C. A., & Nickling, W. G. (2001). The factors influencing the abrasion efficiency of saltating grains on a clay-crusted playa. *Earth Surface Processes and Landforms*, *26*(5), 491–505. https://doi.org/10.1002/esp.193

Huang, Y., Kok, J. F., Martin, R. L., Swet, N., Katra, I., Gill, T. E., et al. (2019). Fine dust emissions from active sands at coastal Oceano dunes, California. *Atmospheric Chemistry and Physics*, *19*(5), 2947–2964. https://doi.org/10.5194/acp-19-2947-2019

Huneeus, N., Chevallier, F., & Boucher, O. (2012). Estimating aerosol emissions by assimilating observed aerosol optical depth in a global aerosol model. *Atmospheric Chemistry and Physics*, *12*(10), 4585–4606. https://doi.org/10.5194/acp-12-4585-2012

Huneeus, N., Schulz, M., Balkanski, Y., Griesfeller, J., Prospero, J., Kinne, S., et al. (2011). Global dust model intercomparison in AeroCom phase I. *Atmospheric Chemistry and Physics*, *11*(15), 7781–7816. https://doi.org/10.5194/acp-11-7781-2011

Jerolmack, D. J., & Brzinski, T. A. (2010). Equivalence of abrupt grain-size transitions in alluvial rivers and eolian sand seas: A hypothesis. *Geology*, *38*(8), 719–722. https://doi.org/10.1130/G30922.1

Jerolmack, D. J., Reitz, M. D., & Martin, R. L. (2011). Sorting out abrasion in a gypsum dune field. *Journal of Geophysical Research*, *116*, F02003. https://doi.org/10.1029/2010JF001821

Jickells, T. D., An, Z. S., Andersen, K. K., Baker, A. R., Bergametti, G., Brooks, N., et al. (2005). Global iron connections between desert dust, ocean biogeochemistry, and climate. *Science*, *308*(5718), 67–71. https://doi.org/10.1126/science.1105959

Katra, I., Yizhaq, H., & Kok, J. F. (2014). Mechanisms limiting the growth of aeolian megaripples. *Geophysical Research Letters*, *41*, 858–865. https://doi.org/10.1002/2013GL058665

Katra, I., Gross, A., Swet, N., Tanner, S., Krasnov, H., & Angert, A. (2016). Substantial dust loss of bioavailable phosphorus from agricultural soils. *Scientific Reports*, *6*(1), 1, 24736–7. https://doi.org/10.1038/srep24736

Khalaf, F. I., & Gharib, I. M. (1985). Roundness parameters of quartz grains of recent aeolian sand deposits in Kuwait. *Sedimentary Geology*, *45*(1–2), 147–158. https://doi.org/10.1016/0037-0738(85)90028-4

Klose, M., & Shao, Y. (2013). Large-eddy simulation of turbulent dust emission. *Aeolian Research*, *8*, 49–58. https://doi.org/10.1016/j.aeolia.2012.10.010

Knippertz, P., & Todd, M. C. (2012). Mineral dust aerosols over the Sahara: Meteorological controls on emission and transport and implications for modeling. *Reviews of Geophysics*, *50*, RG1007. https://doi.org/10.1029/2011RG000362

Kok, J. F., Mahowald, N. M., Fratini, G., Gillies, J. A., Ishizuka, M., Leys, J. F., et al. (2014). An improved dust emission model—Part 1: Model description and comparison against measurements. *Atmospheric Chemistry and Physics*, *14*(23), 13023–13041. https://doi.org/10.5194/acp-14-13023-2014

Kok, J. F., Parteli, E. J. R., Michaels, T. I., & Karam, D. B. (2012). The physics of wind-blown sand and dust. *Reports on Progress in Physics*, *75*(10), 106901. https://doi.org/10.1088/0034-4885/75/10/106901

Kok, J. F., Ridley, D. A., Zhou, Q., Miller, R. L., Zhao, C., Heald, C. L., et al. (2017). Smaller desert dust cooling effect estimated from analysis of dust size and abundance. *Nature Geoscience*, *10*(4), 274–278. https://doi.org/10.1038/ngeo2912

Kok, J. F., Ward, D. S., Mahowald, N. M., & Evan, A. T. (2018). Global and regional importance of the direct dust-climate feedback. *Nature Communications*, *9*(1), 241–211. https://doi.org/10.1038/s41467-017-02620-y

Krasnov, H., Katra, I., Novack, V., Vodonos, A., & Friger, M. D. (2015). Increased indoor PM concentrations controlled by atmospheric dust events and urban factors. *Building and Environment*, *87*, 169–176. https://doi.org/10.1016/j.buildenv.2015.01.035

Kuenen, P. H. (1960). Experimental abrasion 4: Eolian action. *The Journal of Geology*, *68*(4), 427–449. https://doi.org/10.1086/626675

Lancaster, N., Baker, S., Bacon, S., & McCarley-Holder, G. (2015). Owens Lake dune fields: Composition, sources of sand, and transport pathways. *Catena*, *134*, 41–49. https://doi.org/10.1016/j.catena.2015.01.003

Martin, R. L., & Kok, J. F. (2018). Distinct thresholds for the initiation and cessation of aeolian saltation from field measurements. *Journal of Geophysical Research: Earth Surface*, *123*, 1546–1565. https://doi.org/10.1029/2017JF004416

McKenna Neuman, C., Boulton, J. W., & Sanderson, S. (2009). Wind tunnel simulation of environmental controls on fugitive dust emissions from mine tailings. *Atmospheric Environment*, *43*(3), 520–529. https://doi.org/10.1016/j.atmosenv.2008.10.011

Muhs, D. R. (2004). Mineralogical maturity in dunefields of North America, Africa and Australia. *Geomorphology*, *59*(1-4), 247–269. https://doi.org/10.1016/j.geomorph.2003.07.020

Muhs, D. R., Budahn, J. R., Johnson, D. L., Reheis, M., Beann, J., Skipp, G., et al. (2008). Geochemical evidence for airborne dust additions to soils in Channel Islands National Park, California. *GSA Bulletin*, *120*(1–2), 106–126. https://doi.org/10.1130/B26218.1

Nenes, A., Murray, B., & Bougiatioti, A. (2014). Mineral dust and its microphysical interactions with clouds. In P. Knippertz, & J.-B. W. Stuut (Eds.), *Mineral dust: A key player in the Earth system*, (pp. 287–325). Dordrecht: Springer Netherlands. https://doi.org/10.1007/978-94-017-8978-3_12

Nesbitt, H. W., Fedo, C. M., & Young, G. M. (1997). Quartz and feldspar stability, steady and non-steady-state weathering, and petrogenesis of siliciclastic sands and muds. *The Journal of Geology*, *105*(2), 173–192. https://doi.org/10.1086/515908

Nesbitt, H. W., & Young, G. M. (1984). Prediction of some weathering trends of plutonic and volcanic rocks based on thermodynamic and kinetic considerations. *Geochimica et Cosmochimica Acta*, *48*(7), 1523–1534. https://doi.org/10.1016/0016-7037(84)90408-3

Powers, M. C. (1953). A new roundness scale for sedimentary particles. *Journal of Sedimentary Research*, *23*(2), 117–119. https://doi.org/10.1306/D4269567-2B26-11D7-8648000102C1865D

Pye, K., & Tsoar, H. (1990). *Aeolian sand and sand dunes*. Springer Netherlands. Retrieved from https://www.springer.com/gp/book/9789401159883, DOI: https://doi.org/10.1007/978-94-011-5986-9

Pye, K., & Tsoar, H. (2009). *Aeolian sand and sand dunes*. Berlin, Heidelberg: Springer Berlin Heidelberg. https://doi.org/10.1007/978-3-540-85910-9

Roskin, J., Katra I., Blumberg D. G. (2014). Particle-size fractionation of eolian sand along the Sinai-Negev erg of Egypt and Israel. *Geological Society of America Bulletin*, *126*, (1-2), 47–65. https://doi.org/10.1130/b30811.1

Rousé, P. C., Fannin, R. J., & Shuttle, D. A. (2008). Influence of roundness on the void ratio and strength of uniform sand. *Géotechnique*, *58*(3), 227–231. https://doi.org/10.1680/geot.2008.58.3.227

Schmerler, E., Katra, I., Kok, J. F., Tsoar, H., & Yizhaq, H. (2016). Experimental and numerical study of Sharp's shadow zone hypothesis on sand ripple wavelength. *Aeolian Research*, *22*, 37–46. https://doi.org/10.1016/j.aeolia.2016.05.006

Shao, Y., Ishizuka, M., Mikami, M., & Leys, J. F. (2011). Parameterization of size-resolved dust emission and validation with measurements. *Journal of Geophysical Research*, *116*, D08203. https://doi.org/10.1029/2010JD014527

Smith, B. J., Wright J. S., Whalley W. B. (1991). Simulated aeolian abrasion of Pannonian sands and its implications for the origins of Hungarian loess. *Earth Surface Processes and Landforms*, *16*, (8), 745–752. https://doi.org/10.1002/esp.3290160808

Sweeney, M. R., Lu, H., Cui, M., Mason, J. A., Feng, H., & Xu, Z. (2016). Sand dunes as potential sources of dust in northern China. *Science China Earth Sciences*, *59*(4), 760–769. https://doi.org/10.1007/s11430-015-5246-8

Swet, N., Elperin, T., Kok, J. F., Martin, R. L., Yizhaq, H., & Katra, I. (2019). Can active sands generate dust particles by wind-induced processes? *Earth and Planetary Science Letters*, *506*, 371–380. https://doi.org/10.1016/j.epsl.2018.11.013

Swet, N., & Katra, I. (2016). Reduction in soil aggregation in response to dust emission processes. *Geomorphology*, *268*, 177–183. https://doi.org/10.1016/j.geomorph.2016.06.002

Thomas, D. S. G. (1987). The roundness of aeolian quartz sand grains. *Sedimentary Geology*, *52*(1-2), 149–153. https://doi.org/10.1016/0037-0738(87)90020-0

Vodonos, A., Friger, M., Katra, I., Krasnov, H., Zahger, D., Schwartz, J., & Novack, V. (2015). Individual effect modifiers of dust exposure effect on cardiovascular morbidity. *PLoS ONE*, *10*(9), e0137714. https://doi.org/10.1371/journal.pone.0137714

Wadell, H. (1932). Volume, shape, and roundness of rock particles. *The Journal of Geology*, *40*(40), 443–451. https://doi.org/10.1086/623964

Welti, A., Lohmann, U., & Kanji, Z. A. (2019). Ice nucleation properties of K-feldspar polymorphs and plagioclase feldspars. *Atmospheric Chemistry and Physics*, *19*(16), 10901–10918. https://doi.org/10.5194/acp-19-10901-2019

Whalley, W. B., Marshall, J. R., & Smith, B. J. (1982). Origin of desert loess from some experimental observations. *Nature*, *300*(5891), 433–435. https://doi.org/10.1038/300433a0

Whalley, W. B., Smith, B. J., McAlister, J. J., & Edwards, A. J. (1987). Aeolian abrasion of quartz particles and the production of silt-size fragments: Preliminary results. *Geological Society, London, Special Publications*, *35*(1), 129–138. https://doi.org/10.1144/gsl.sp.1987.035.01.09

Wright, J., Smith, B., & Whalley, B. (1998). Mechanisms of loess-sized quartz silt production and their relative effectiveness: Laboratory simulations. *Geomorphology*, *23*(1), 15–34. https://doi.org/10.1016/S0169-555X(97)00084-6

Zender, C. S., Bian, H., & Newman, D. (2003). Mineral Dust Entrainment and Deposition (DEAD) model: Description and 1990s dust climatology. *Journal of Geophysical Research*, *108*(D14), 4416. https://doi.org/10.1029/2002JD002775

Zobeck, T. M., & Van Pelt, R. S. (2006). Wind-induced dust generation and transport mechanics on a bare agricultural field. *Journal of Hazardous Materials*, *132*(1), 26–38. https://doi.org/10.1016/j.jhazmat.2005.11.090